2018 24th International Conference on Pattern Recognition (ICPR)
Beijing, China, August 20-24, 2018

A Method for PET-CT Lung Cancer Segmentation based on Improved Random Walk

Zhe Liu*, Yuqing Song*, Charlie Maere*, Qingfeng Liu*, Yan Zhu†, Hu Lu* and Deqi Yuan‡
*School of Computer Science and Communication Engineering
Jiangsu University
Zhenjiang, Jiangsu Province, China 212013
Email: 1000004088@ujs.edu.cn
†Affiliated Hospital of Jiangsu University
Jiangsu University
Zhenjiang, Jiangsu Province, China 212013
‡Zhenjiang First People's Hospital Branch
Zhenjiang, Jiangsu Province, China 212013

***Abstract*—Segmentation methods only work for a single imaging modality usually suffer from the low spatial resolution in positron emission tomography (PET) or low contrast in computed tomography (CT) when the tumor region is inhomogeneous or not obvious. To address this problem, we develop a segmentation method combining the advantages and disadvantages of PET and CT. Firstly, the initial contours are obtained by the pre-segmentation of PET images using region growing and mathematical morphology. The initial contours can be used to automatically obtain the seed points required for random walk on PET and CT images, at the same time, they can be also used as a constraint in the random walk on CT images to solve the shortcoming that the tumor areas are not obvious if the CT images have not been enhanced. For the reason that CT provides essential details on anatomic structures, the anatomic structures of CT can be used to improve the weight of random walk on PET images. Finally, the similarity matrices obtained by random walk on PET and CT images are weighted to obtain identical results on PET and CT images. Our methods achieve an average DSC of 0.8456 $\pm$ 0.0703 on 14 patients with lung cancer. Our method has much better performance when the tumors are inhomogeneous on PET images and not obvious on CT images.**

***keywords*—Multi-modal medical image; Image segmentation; Random walk.**

I. Introduction

Lung cancer is one of the major causes of death from cancers. The exact segmentation of lung tumors can accurately detect the location and contour, it also plays an important role during the early diagnosis of lung cancer. Clinical lung tumor segmentation is mainly determined by radiologist, however, the accuracy of segmentation is always depended on radiologist's clinical experience. Therefore, the development of lung tumor precise segmentation technology is extremely important.

For effective assessment of target volumes in cancer treatment, medical imaging modalities like CT and PET are widely used. In recent years, the tumor segmentation based on PET and CT images has attracted considerable attention. Xiaopeng Wang et al proposed a method based on support vector machine (SVM) and improved level set model to deal with the fuzzy edges of tumors caused by the complex relationship between tumors and tissues[1]. The methods most widely used to do tumor segmentation on PET images in clinical practice is threshold based on standardized uptake value (SUV), such as using an absolute SUV values [2], [3], a percentage of the maximum SUV [4]. CT images usually have high spatial resolution and provide detailed anatomical information. However, limited functional information of organs and tissues can be captured from CT imaging [5]. In order to distinguish malignant tumors from normal tissues more easily, PET imaging was introduced, in which target tumors have high SUV. However, due to the limitation of imaging technology, PET images usually have low spatial resolution means that the boundary of target tumor can be fuzzy and indistinct [6]. Thus, the accuracy of image segmentation based on single modal is often unsatisfactory. Combined PET-CT scanners can provide complementary functional information and anatomical information from a single scanning session. A large number of studies have demonstrated that combing PET and CT information results in more consistent delineation of tumor volumes[7], [8], [9], [10], [11]. Some PET-CT segmentation methods have been developed, which have achieved much more accurate segmentation results compared to those segmentation methods based on PET or CT. Wei Ju et al integrated random walk and graph cut to make full use of the superior contrast of PET images and superior spatial resolution of CT images, in which random walk was utilized as an initialization tool. The co-segmentation problem was formulated as an energy minimization problem [7]. Ulas Bagci et al reported that they unified the domains of anatomical and functional images, represented them in a product lattice, and performed simultaneous delineation of regions based on random walk image segmentation. They also proposed an effective seed localization method to make the proposed segmentation process full automatic [8].

In this paper, we improve the random walk to make full use of complementary functional information and anatomical information of PET-CT images. The proposed method obtain the initial contours by the pre-segmentation of PET images, the

978-1-5386-3787-6/18/$31.00 ©2018 IEEE

initial contours can be used to effectively locate the seed points required for random walk of PET and CT images. For CT segmentation, due to the limited functional information of CT images, the target tumor can hardly be distinguished from the normal area, the initial contours can act as a constraint to guide the segmentation on the CT images. For PET segmentation, the essential details on anatomic structures that CT images provide are incorporated into the weights of random walk on the PET images to further improve the accuracy of segmentation. Finally, the similarity matrices obtained by random walk on PET and CT images are weighted to obtain identical results on PET and CT images.

II. Random walk

Random walk maps an image $I = \{x_1, \ldots, x_i, \ldots, x_N\}$ into a connected and undirected graph *G(V,E)*, where each node $v_i \in V$ in the graph represents each pixel in the image. $e_{ij} \in E \subset V \times V$ is an edge connecting node v_i and its neighborhood v_j with a weight ω, ω represents the probability of random walker passing through this edge. The weighting function we employed is the typical Gaussian function derived from the suggested in [12]:

$$\omega_{ij} = \exp(-\beta(v_i - v_j)^2) \tag{1}$$

Random walk algorithm requires interactive input of seeds, the nodes in the graph can be divided into two sets. One set is those nodes which are defined by user, the other is unknown nodes. The segmentation problem is to calculate the probability of all unlabeled seeds to the labeled seed points. Grady has proved that the desired probabilities has the same solution as the combinatorial Dirichlet problem [12], [13]. The formulation of Dirichlet integral is stated as:

$$D[x] = \frac{1}{2}x^T L x = \frac{1}{2}\sum_{e_{ij}\in E}\omega_{ij}(x_i - x_j)^2 \tag{2}$$

where x denotes the probability of each voxel, L represents the combinatorial Laplacian matrix. The matrix is stated as:

$$L_{ij} = \begin{cases} d_i, & if\ i = j, \\ -\omega_{ij}, & if\ v_i\ and\ v_j\ are\ adjacent\ nodes, \\ 0, & others \end{cases} \tag{3}$$

where $d_i = \sum w_{ij}$ represents the weights of all nodes adjacent to v_i. Random walk divides all nodes into two sets, so the matrix L can be represented as:

$$L = \begin{bmatrix} L_M & B \\ B^T & L_N \end{bmatrix} \tag{4}$$

where L_M represents the weight matrix of labeled nodes, L_N represents the weight matrix of unlabeled nodes, *B* represents the weight matrix between labeled nodes and unlabeled nodes. After a series of operations, the optimal solution of Dirichlet integral can be represented as:

$$L_N X = -B^T M \tag{5}$$

where X is the probability matrix required. Based on the similarity probability matrices, we can achieve the final segmentation result.

III. Proposed Methods

A. PreProcessing

The images collected in this paper are from combined PET-CT scanner. PET and CT images are acquired nearly at the same time and the possibility of deformation of the organ during the shooting process is very small. However, PET images resolution and CT resolution are not the same due to the difference between PET and CT imaging technology. The proposed method needs to keep a one-to-one voxel correspondence between the CT and PET images. So, we need a preprocessing. Firstly, the PET image is up sampled using a cubic B-spline interpolator to make the PET and CT images have same resolution. Secondly, the PET image is registered with the CT image using rigid transformation. Affine registration is frequently used by physicians for PET-CT delineation of tumor volumes, for simplicity, we choose to use affine transformation in this research [14], [15]. Fig.1 shows the original CT image and the corresponding PET after up sampling, two images of the overlay display before registering and two images of the overlay display after registering.

B. Seed localization algorithm

The current random walk segmentation mostly depends on interactive input of seeds. Interactive method of input of seeds makes a certain request for the person who chooses the seed points. So we propose an automatic seeding algorithm based on region growing and mathematical morphology. On PET images, lung tumors can be distinguished as hot spots due to their high intensities representing the voxel activities. SUV provides a semi-quantitative measurement to normalize PET intensities across different acquisition times and varying patients. In this paper, we choose region growing to make a pre-segmentation to obtain the initial profile of the tumor. Region growing has been proved that it has a certain degree of accuracy when performing tumor segmentation on PET images [8]. The reason that we choose region growing rather than fixed threshed is to avoid segmentation leakage into surrounding tissues with similar PET tracer uptake. The seed localization procedure is as follows:

(1) SUV is used to measure the metabolism of various tissues and organs. The tumor area is more metabolic than normal, so we choose the pixel point with the largest SUV value as the initial seed point of the region growing.

(2) Search for neighborhoods in 8 directions around the initial seed point that meet the following criteria:

$$a_i = \begin{cases} 1, & if\ SUV(v_i) > 50\%SUV_{MAX}, \\ 0, & otherwise \end{cases} \tag{6}$$

this criteria is set according to the current experience of knowledge. Based on prior knowledge, it is highly possible that the voxels having SUV higher than 50% of maximum SUV belong to the tumor [16].

(3) If the characteristic of seed point does not satisfy equation (6), region growing is completed. The obtained segmentation results need to deal with mathematical morphology to acquire the initial tumor contour.

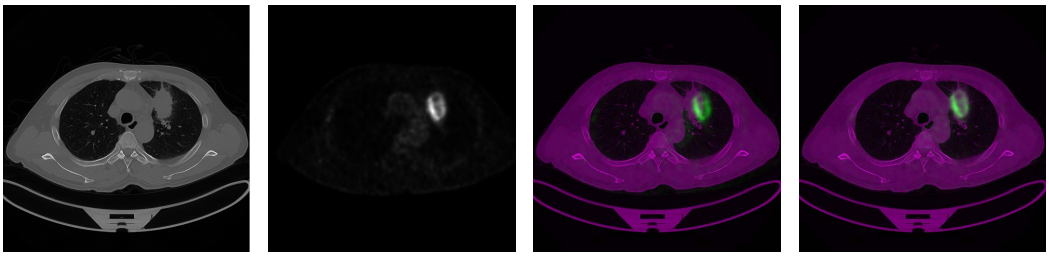

(a) (b) (c) (d)

Fig. 1: The register process. (a) the original slice of CT. (b) the slice of PET after up sampling. (c) the overplay display of two images before registering. (d) the overplay display of two images after registering.

(4) Use the pseudo Monte Carlo algorithm to select foreground seed points in the initial contour.
(5) Search for the 8 neighborhoods of each foreground seed point to select those points satisfying the following formula as the background seeds:

$$a_j = \begin{cases} 1, & if\ SUV(v_i) < 5\%SUV_{MAX}, \\ 0, & otherwise \end{cases} \tag{7}$$

this formula is also based on prior knowledge, it is highly possible that the voxels having SUV lower than 15% of maximum SUV belong to the normal area [7], in this paper we choose 5% of maximum SUV as threshold. Map those seeds onto CT images to obtain seeds of CT images when we acquire the foreground and background seeds of PET images.

C. Random walk on CT image

CT images usually provide enough structural information of the organs and tissues but little functional information. Tumor area can hardly be distinguished from the normal area on the non-enhanced CT images. CT images acquired from combined PET-CT scanners usually are non-enhanced. Random walk can hardly obtain the accurate tumor area from the non-enhanced CT, so we add a constraint to random walk on the CT images. The initial tumor contour obtained by the pre-segmentation of seed localization algorithm is treated as a constraint, the probability that the random walker walks within the constraint is greater than the external region.

After pre-processing, PET and CT images are considered to have achieved a one-to-one correspondence between the pixels within the images. So the initial contours obtained on the PET images are mapped onto the CT images. In the initial contours, the random walker walks with the normal weight, the area outside the initial contour may belong to the lesion area, but the probability that the random walker passes through these areas should be less than the initial contour. In this paper, we enclose the initial contour with the smallest enclosing circle, the area of the smallest enclosing circle but outside the initial contour is considered as suspected lesion area. Calculate the Euclidean distance between two adjacent nodes in the suspected lesion area and the center of initial contour, select the value obtained by dividing the smaller value and the radius of the minimum circumference circle as the weight of edge between the two adjacent nodes. The area outside the smallest enclosing circle is considered to be the normal area, the weight of this area is set to 0.01, the reason of not to set 0 is to prevent the process of solving the Laplacian matrix singularity without solution. The constraint function has the following form:

$$a_{ij} = \begin{cases} 0, & v_i = v_j, \\ 0.01, & (v_i, v_j) \notin \boldsymbol{C} \\ \gamma \cdot \omega_{ij}, & v_i \neq v_j\ \&\ (v_i, v_j) \notin \boldsymbol{E}\ \&\ (v_i, v_j) \in \boldsymbol{C} \\ \omega_{ij}, & v_i \neq v_j\ \&\ (v_i, v_j) \in \boldsymbol{E} \end{cases} \tag{8}$$

where $\boldsymbol{E}$ is the initial contour mapped on the CT image, $\boldsymbol{C}$ represents the smallest enclosing circle. γ represents the added constraint item, it takes this form:

$$\gamma = \rho(exp(-\frac{p}{r})) \tag{9}$$

where r is the radius of the smallest enclosing circle, p represents the smaller Euclidean distance between the adjacent node and the center of the initial contour:

$$p = min(||v_i, O||, ||v_j, O||) \tag{10}$$

where O denotes the center of the initial, v_i and v_j represents the adjacent node located in the initial contour. Fig.2 shows the effects of the constraint on CT.

D. Random walk on PET images

Due to the low resolution of PET images, the partial volume effect is more serious than CT images. The tumor area on the PET image is usually heterogeneous. The location of the tumor on the PET image is clear but the tumor profile is fuzzy and indistinct, CT image usually provides detailed anatomical information. So we extract the gradient information of the CT image and map it onto the PET image to improve the weight of random walk:

$$\omega_{ij} = exp(-\alpha(v_i - v_j)^2 - \beta(g_i - g_j)^2) \tag{11}$$

where v_i denotes the SUV values in the PET images, g_i is the gradient feature extracted from the CT image.

E. Similarity matrix weighting

The probability matrix obtained from the random walk on PET image and the probability matrix obtained from the random walk on CT image are weighted to obtain the

(a) (b) (c) (d) (e)

Fig. 2: The effect of CT constraint. (a) One CT slice. (b) The corresponding PET slice. (c) The ground truth. (d) The original probability map of random walk on CT. (e) The probability map of random walk with constraint.

final probability matrix. The segmentation can be completed according to the final matrix:

$$P = \eta \cdot P_{PET} + \mu \cdot P_{CT} \tag{12}$$

η and μ respectively represent the weights of the probability matrix obtained from random walk on PET and CT images.

IV. Results

A. Datasets

Our segmentation approach was evaluated in a data set which consists of 14 PET-CT images obtained from different patients with lung tumors. Each set of images contains one CT image and one corresponding PET image. Images are acquired with a dual PET and CT scanner developed by Siemens Medical Solutions USA. For each slice of PET images, the reconstructed matrix size is $200 \times 200 \times 60$. The reconstructed matrix size for each CT slice is $512 \times 512 \times 60$. After the preprocessing step, PET images have exactly the same size as the corresponding CT images and the CT and PET images nearly keep a one-to-one voxel correspondence. The standard tumor contours were delineated by two experts manually on the PET images with the guidance of the corresponding CT images.

B. Comparison methods

To evaluate the performance of the proposed method, we compare it with other methods, including: 1) a threshold of 40% maximum SUV on PET (referred to as fixed40%), 2) a threshold of 50% maximum SUV on PET (referred to as fixed50%), 3) an iterative threshold method on PET (referred to as ITM) [17], 4) a region growing method on PET (referred to as RG)[18], 5) a random walk method on PET (referred to as RW)[12]. Due to the indistinct area of tumor in the CT images, so the results of the comparison of these five methods are the segmentation results on the PET images.

C. Validation methods

To evaluate the accuracy of the proposed method, we calculated the spatial overlap between the segmentation results and GT by DSC(Dice's similarity coefficient). DSC is defined as:

$$DSC(U_1, U_2) = \frac{2|U_1 \cap U_2|}{|U_1| + |U_2|} \tag{13}$$

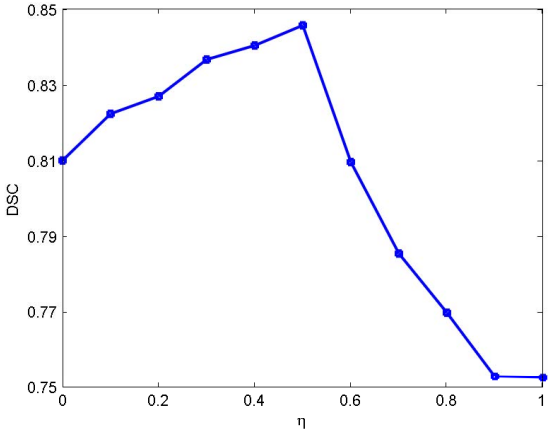

Fig. 3: Averaged DSC obtained by the proposed method with different η values.

where U_1 is the segmented volume, and U_2 denotes the GT volume.

D. Parameter settings

The main parameters referred in our algorithm are most determined empirically. In the random walk on PET, the SUV values plays a more important role than the gradient feature extracted from the CT image, so we set $\alpha = 0.6$,$\beta = 0.4$.The similarity matrixs obtained by random walk on PET and CT images play the same important roles, so η and μ are both 0.5. Fig.3 shows the accuracy in terms of the averaged DSC by the proposed method with the parameter η.

E. Evaluation of clinical cases

To demonstrate the performance of the proposed method, we compare the proposed method with other five methods. The five methods are all applied to the 14 datasets with identical initialization. The DSC comparison is shown as Fig.4.

Table 1 shows the mean DSC and SD for the proposed method and the five comparative methods. For 14 phantom datasets, we can see the proposed method has the superior performance than other five algorithms. Our method achieves DSC of 0.8456±0.0703.

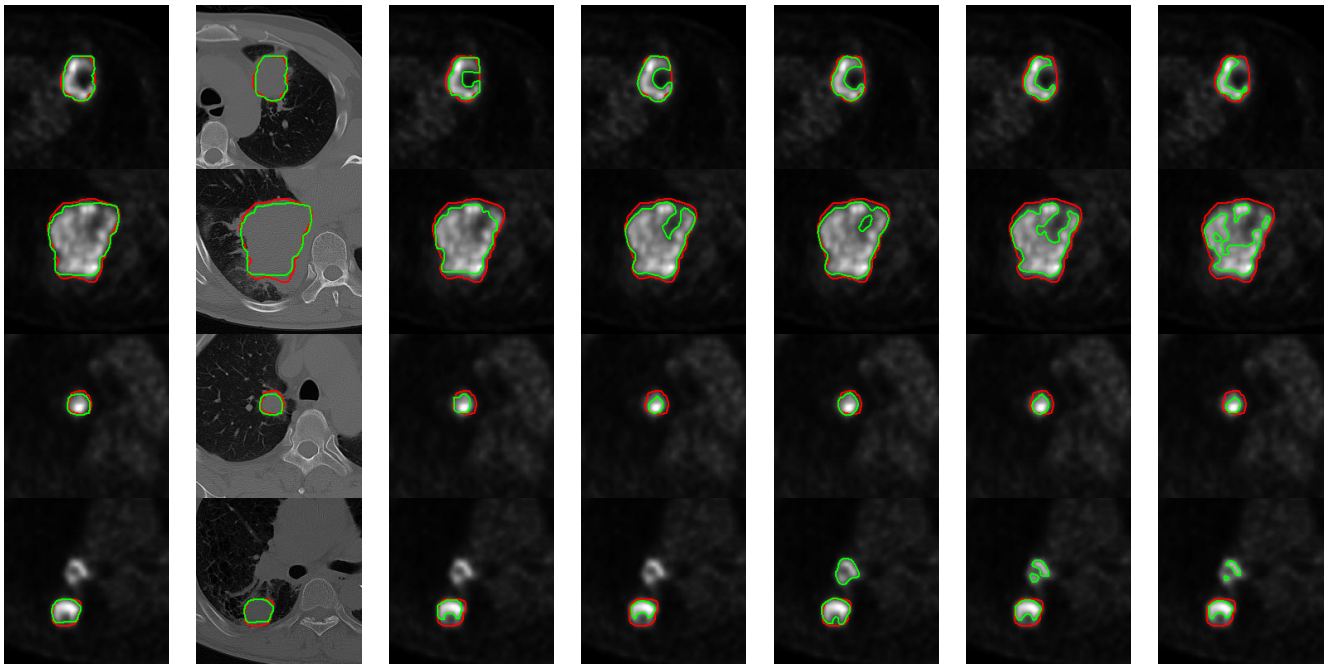

(a) (b) (c) (d) (e) (f) (g)

Fig. 5: Four typical comparative segmentation results of lesions are shown in each column. The segmentation results (green) and ground truth (red) are overlaid. (a) the results on PET images conducted by our proposed method. (b) the results on CT images conducted by our proposed method. (c) segmentation results conducted by random walk solely on PET images. (d) segmentation results conducted by region growing solely on PET images. (e) segmentation results conducted by iterative threshold method solely on PET images. (f) the results conducted by a threshold of 40% SUVmax solely on PET images. (g) the results conducted by a threshold of 50% SUVmax solely on PET images.

TABLE I: The quantitative comparison between the proposed algorithm and the other five algorithms.

Rank	Methods	DSC(mean±SD)
1	Fixed40%	0.6339±0.1145
2	Fixed50%	0.5206±0.1210
3	ITM	0.6694±0.2737
4	RG	0.6819±0.1408
5	RW	0.7237±0.0848
6	Proposed	0.8456±0.0703

The main contribution of the proposed method is that the result of pre-segmentation acts as a constraint during the random walk on CT image, it can make full use of the detailed functional information of PET images. The constraint of PET plays a critical role when the tumor boundary of CT images is not obvious. The tumor area on PET images may contain some necrotic areas (SUV of necrotic areas is usually lower) or the SUV of PET image is heterogeneous due to the inhomogeneous tumor area, in such instances, solely depending on PET leads to leakage to the contour of tumor. So we consider to combine the anatomical information to achieve the accurate boundary. Fig.5 shows the comparison between the proposed algorithm and the other five algorithms on four typical slices. The first image shows that the SUV of tumor on PET image is inhomogeneous and the region of tumor on CT image is not obvious; the second shows that the SUV of tumor of PET image is also inhomogeneous and we can hardly detect the region of tumor from CT image; the tumor region of third image is small, the SUV of PET is much more homogeneous and the tumor region on CT is obvious; the tumor of forth image is involved the chest wall. We can find that our method can achieve much better performance when the SUV of tumor area on the PET is inhomogeneous and the tumor area on CT is not very obvious from the first and second image. We can also notice that the segmentation result is much more accurate when the tumor area on CT and PET is relatively clear from the third image. Our method also achieve a good result when the tumor is involved the chest wall.

V. Conclusion

Traditional medical segmentation methods are usually based on single modal medical images: PET, CT or MR. CT and MR images have high spatial resolution with limited functional information, PET images provide quantitative information about disease and structures with lower spatial resolution than CT or MR. Those segmentation methods based on signal modal image can hardly achieve satisfactory results in the case that the region of tumor is complex. PET-CT images provide complementary functional and anatomical information

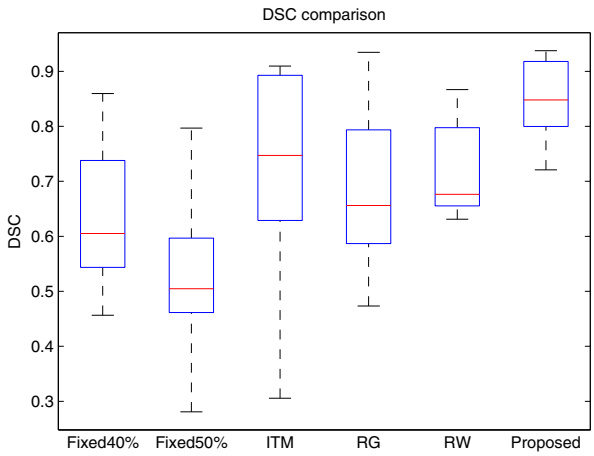

Fig. 4: DSC comparison of the proposed method to traditional methods.

of organs. The segmentation based on PET-CT can make use of advantages of both medical imaging modalities to achieve an accurate outline of the tumor area. We propose a new multi-modal lung tumor image segmentation method, which combines the complementary functional information and anatomical information from PET and CT images. There are also some limitations in our study. The PET and CT images used in our method need to obtain a nearly one-to-one voxel correspondence. We are aware that deformations due to breathing often require nonlinear registration. However, nonlinear registration is complex, for simplicity, the PET and CT images used in our method are those with no non-rigid deformation or slight non-rigid deformation. This process is completed by radiologist. In case that PET and CT images are serious non-rigid deformation, the proposed method is difficult to accurately detect the region of tumor region. The future improvement of our algorithm is to keep the segmentation accuracy and stability when PET and CT images are serious non-rigid deformation. We evaluate our method by DSC. The results show that our method can segment the tumor area more accurately and stably than other traditional segmentation methods.

VI. Acknowledgments

This work was supported by the National Natural Science Foundation of China (61772242, 61572239); Research Fund for Advanced Talents of Jiangsu University (14JDG141); China Postdoctoral Science Foundation (2017M611737); Zhenjiang Health and Family Planning Science and Technology Project (SHW2017019); Zhenjiang Social Development Project (SH2016029).

References

[1] Xiao peng Wang, Wen Zhang, and Ying Cui. Tumor segmentation in lung ct images based on support vector machine and improved level set. *Optoelectronics Letters*, 11(5):395–400, 2015.

[2] Robert Hong, James Halama, Davide Bova, Anil Sethi, and Bahman Emami. Correlation of pet standard uptake value and ct window-level thresholds for target delineation in ct-based radiation treatment planning. *International Journal of Radiation Oncology Biology Physics*, 67(3):720–726, 2007.

[3] C Scarfone, W. C. Lavely, A. J. Cmelak, D Delbeke, W. H. Martin, D Billheimer, and D. E. Hallahan. Prospective feasibility trial of radiotherapy target definition for head and neck cancer using 3-dimensional pet and ct imaging. *Journal of Nuclear Medicine*, 45(4):543–52, 2004.

[4] T. R. Miller and P. W. Grigsby. Measurement of tumor volume by pet to evaluate prognosis in patients with advanced cervical cancer treated by radiation therapy. *International Journal of Radiation Oncology Biology Physics*, 53(2):353–9, 2002.

[5] Baardwijk A Van, G Bosmans, L Boersma, J Buijsen, S Wanders, M Hochstenbag, R. J. van Suylen, A Dekker, C Dehingoberije, and R Houben. Pet-ct-based auto-contouring in non-small-cell lung cancer correlates with pathology and reduces interobserver variability in the delineation of the primary tumor and involved nodal volumes. *International Journal of Radiation Oncology Biology Physics*, 68(3):771–8, 2007.

[6] R Boellaard, N. C. Krak, O. S. Hoekstra, and A. A. Lammertsma. Effects of noise, image resolution, and roi definition on the accuracy of standard uptake values: a simulation study. *Journal of Nuclear Medicine Official Publication Society of Nuclear Medicine*, 45(9):1519, 2004.

[7] W. Ju, D. Xiang, B. Zhang, L. Wang, I Kopriva, and X. Chen. Random walk and graph cut for co-segmentation of lung tumor on pet-ct images. *IEEE Transactions on Image Processing*, 24(12):5854–5867, 2015.

[8] Ulas Bagci, Jayaram K. Udupa, Neil Mendhiratta, Brent Foster, Ziyue Xu, Jianhua Yao, Xinjian Chen, and Daniel J. Mollura. Joint segmentation of anatomical and functional images: Applications in quantification of lesions from pet, pet-ct, mri-pet, and mri-pet-ct images. *Medical Image Analysis*, 17(8):929–945, 2013.

[9] Q. Song, J. Bai, D. Han, S Bhatia, W. Sun, W Rockey, J. E. Bayouth, J. M. Buatti, and X. Wu. Optimal co-segmentation of tumor in pet-ct images with context information. *IEEE Transactions on Medical Imaging*, 32(9):1685–1697, 2013.

[10] Hui Cui, Xiuying Wang, Weiran Lin, Jianlong Zhou, Stefan Eberl, Dagan Feng, and Michael Fulham. Primary lung tumor segmentation from petcct volumes with spatialctopological constraint. *International Journal of Computer Assisted Radiology and Surgery*, 11(1):1–11, 2015.

[11] H. Mi, C Petitjean, P Vera, and S Ruan. Joint tumor growth prediction and tumor segmentation on therapeutic follow-up pet images. *Medical Image Analysis*, 23(1):84–91, 2015.

[12] Leo Grady. Random walks for image segmentation. *IEEE Transactions on Pattern Analysis and Machine Intelligence*, 28(11):1768–1783, 2006.

[13] L Grady, T Schiwietz, S Aharon, and R Westermann. Random walks for interactive organ segmentation in two and three dimensions: implementation and validation. *Medical Image Computing and Computer-Assisted Intervention C MICCAI 2005*, 8(8):773–780, 2005.

[14] Y. E. Erdi, K Rosenzweig, A. K. Erdi, H. A. Macapinlac, Y. C. Hu, L. E. Braban, J. L. Humm, O. D. Squire, C. S. Chui, and S. M. Larson. Radiotherapy treatment planning for patients with non-small cell lung cancer using positron emission tomography (pet). *Radiotherapy and Oncology*, 62(1):51–60, 2002.

[15] G. W. Goerres, E Kamel, T. N. Heidelberg, M. R. Schwitter, C Burger, and G. K. von Schulthess. Pet-ct image co-registration in the thorax: influence of respiration. *European Journal of Nuclear Medicine and Molecular Imaging*, 29(3):351–360, 2002.

[16] H Zaidi and Naqa I El. Pet-guided delineation of radiation therapy treatment volumes: a survey of image segmentation techniques. *European Journal of Nuclear Medicine and Molecular Imaging*, 37(11):2165–2187, 2010.

[17] Laura Drever, Wilson Roa, Alexander Mcewan, and Don Robinson. Iterative threshold segmentation for pet target volume delineation. *Medical Physics*, 34(4):1253–1265, 2007.

[18] Yu Bu Lee, Soo Min Song, Jae Sung Lee, and Myoung Hee Kim. Tumor segmentation from small animal pet using region growing based on gradient magnitude. In *International Workshop on Enterprise NETWORKING and Computing in Healthcare Industry, 2005. Healthcom*, pages 243–247, 2005.